# Determining Reflectance Properties of an Object Using Range and Brightness Images

Katsushi Ikeuchi, *Member, IEEE,* and Kosuke Sato, *Member, IEEE*

*Abstract*— **This paper discusses a method of recovering reflectance properties of a surface from a range image given by a range finder and a brightness image given by a standard TV camera. We will use the Torrance-Sparrow model for our reflectance model. The model consists of the Lambertian and specular components; its reflectance properties consist of relative strength between the Lambertian and specular components and specular sharpness as well as light source direction. We will employ an iterative least square fitting method to obtain these parameters based on the range and brightness images. Using the obtained parameters, we segment an input image into four different parts: Lambertian reflection, specular reflection, interreflection, and shadow part. We will also reconstruct ideal images that consist of only Lambertian or specular reflection.**

*Index Terms*— **Image reconstruction, Lambertian reflection, least square fitting, reflectance map, segmentation, specular reflection, Torrance-Sparrow model.**

## I. Introduction

MEASURING surface reflectance properties from image brightness is an important issue in both basic and applied computer vision research. For example, in basic computer vision research, surface reflectance properties give a reliable cue for segmenting images, and we can build a more dependable and accurate segmentation system using surface reflectance. Since surface reflectance properties are directly related to surface polish and roughness, they are an important inspection criteria in many industrial applications. Currently, tasks such as inspecting surface deformations in silicon wafers or detecting flaws in the painted exteriors of cars are performed by the judgement of the human eye. Since many of these tasks are tedious and potentially dangerous, it is desirable to investigate a method that measures surface reflectance automatically and develop an inspection system based on this method.

Manuscript received April 10, 1991. This research was sponsored by Osaka Gas, Osaka, Japan, and conducted in the Task-Oriented Vision Laboratory, School of Computer Science, Carnegie Mellon University. Image Understanding Research in TVL is supported in part by the Defense Advanced Research Projects Agency, DOD, through DARPA Order 4976, and monitored by the Air Force Avionics Laboratory under contract F33615-87-C-1499. The views and conclusions contained in this document are those of the authors and should not be interpreted as representing the official policies, either expressed or implied, of the Defense Advanced Research Projects Agency or of the U.S. Government.

K. Ikeuchi is with the School of Computer Science, Carnegie Mellon University, Pittsburgh, PA 15213.

K. Sato is with the Faculty of Engineering Science, Osaka University, Osaka, Japan

IEEE Log Number 9101437.

When light strikes an interface between two different media, some percentage of the light passes through the boundary, and the remaining part of the light is reflected. The penetrating light hits internal pigments of an object and is re-emitted randomly. We will refer this randomly reflected component from the inside of an object as the *Lambertian* component, whereas the part reflected on the surface of the object is referred to as the *specular* component.

Although the measurement of the reflectance properties, such as relative strength between the two components or angular distributions of these components, has been the topic of innumerable pieces of literature in applied physics, few attempts have been made to apply these theories and recover the reflectance properties from image brightness in computer vision research. Woodham proposed to recover surface albedo using photometric stereo [17]. Nayar *et al.* proposed to recover relative strength of reflectance components from a sequence of images taken under a collection of extended light sources [10]. Klinker *et al.* proposed to separate specular reflection from Lambertian reflection by analysis of color [8]. Wolff proposed a separation method based on analysis of polarization [16].

Recently, range finders have been widely used in industrial applications [2]. By using such devices, a range image can be obtained relatively easily. Based on a range image and a brightness image given by a standard TV camera, we can recover surface reflectance parameters. This paper describes a method not only to the separate specular reflection component from Lambertian reflection component but also to determine relative strength between the two components.

In order to recover such reflectance properties, we need a solid reflectance understanding on reflectance mechanism. In the field of applied physics, two different approaches have been proposed for modeling the reflectance mechanism. Physical optics is based directly on electromagnetic wave theory and uses Maxwell's equation to study the propagation of light. In particular, Beckmann and Spizzichino [1] formulated a reflectance model by solving Maxwell's equation using the Helmholtz integral while applying Kirchoff's assumption to a perfect conductor surface. On the other hand, geometric optics analyzes a path of light ray that approximates the specular component of reflection. The Torrance-Sparrow model was developed to describe the specular reflection of rough surfaces and, due to its being a simpler mathematical formula, is more popular than the Beckmann-Spizzichino model [15].

Healey and Binford have used the Torrance-Sparrow model to determine local shape from specular reflections [5]. Tagare and deFigueiredo have discussed both the Beckmann-

0162–8828/91$01.00 © 1991 IEEE

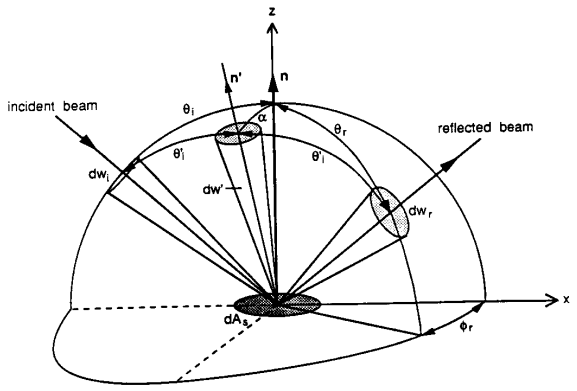


Fig. 1. Geometry for Torrance-Sparrow model [15].

Spizzichino and the Torrance-Sparrow models in their survey of various reflection mechanisms [14]. Nayar *et al.* have proposed an unified reflectance model based on the Beckmann-Spizzichino and Torrance-Sparrow models [11].

We will assume that the wavelength of incident light is far shorter than the physical dimension of the surface imperfection. In this case, the results from the Beckmann-Spizzichino model agrees with those from the Torrance-Sparrow model [11]. Since the Torrance-Sparrow model is simpler than the Beckmann-Spizzichino model, this paper will employ the Torrance-Sparrow reflectance model.

The first section will examine the Torrance-Sparrow reflectance model. Then, we will refine the model into a more specific reflectance model and derive an image irradiance equation that will establish a relationship between surface orientations, reflectance parameters, and image irradiance. Third, we will devise a method that incorporates this equation and estimates the values for the reflectance parameters. Finally, we will extend this methodology to a complete system that recovers reflectance parameters from image brightness and can reconstruct ideal images.

## II. Reflectance Model

### *Torrance-Sparrow Model*

This subsection outlines the demonstration of the Torrance-Sparrow model [15]. Fig. 1 shows the geometry for the model. The surface area $dA_s$ is located at the origin of the coordinate frame, and its surface normal points in the direction of the $Z$ axis. The surface is illuminated by a beam of light that lies in the $X - Z$ plane and is incident on the surface at an angle $\theta_i$. The light source has radiance and solid angle $L_i$ and $d\omega_i$, respectively.

When light strikes on a surface area $dA_s$, some of the light passes through the surface area, and the remaining portion is reflected. Light penetrating the surface area hits internal pigments of an object, is partly absorbed, and is randomly emitted. We will refer to this reflection component as the *Lambertian component*. The incident flux on the surface $d^2\Phi_i$ is given as $L_i d\omega_i dA_s \cos\theta_i$. The surface irradiance $E_s$ is determined by dividing the incident flux by the surface area $dA_s$. Thus

$$E_s = L_{lamb,r} d\omega_i \cos\theta_i.$$

Since $L_r$, which is the surface radiance given by the Lambertian component, is proportional to the irradiance of the surface given by a light source [9] and $K_{lamb}$ is a proportional constant, we can state the following formula:

$$L_{lamb,r} = K_{lamb} L_i d\omega_i \cos\theta_i. \tag{1}$$

This equation is known as Lambertian's cosine law.

The remaining light, which is reflected on the surface, is referred to as the *specular component*. For analyzing the specular component, Torrance and Sparrow have assumed the facet slopes to be normally distributed. Further, they have assumed the distribution to be rotationally symmetric about the mean surface normal $\vec{\mathbf{N}}$. Hence, facet slopes may be represented by a one-dimensional normal distribution:

$$P_\alpha(\alpha) = c\exp(-\frac{\alpha^2}{2\sigma_\alpha^2}) \tag{2}$$

where $c$ is a constant, and the facet slope $\alpha$ represents surface roughness by the mean value $\langle\alpha\rangle$ and the standard deviation $\sigma_\alpha$.

The surface area $dA_s$ is located at the origin of the coordinate system, and its surface normal points in the direction of the $z$ axis. The surface is illuminated by a beam of light that lies in the $xz$ plane and is incident on the surface at angle $\theta_i$. We are interested in determining the radiance of the surface in the direction $(\theta_r, \phi_r)$.

Only planar microfacets having normal vectors within the solid angle $d\omega'$ are capable of specularly reflecting flux that is incident to angle $\theta_i$ into the infinitesimal solid angle $d\omega_r$. The number of facets per unit area of the surface that are oriented within the solid angle $d\omega'$ is equal to $p_\alpha(\alpha)d\omega'$. Therefore, the number of facets in the surface area $dA_s$ that are oriented within $d\omega'$ is equal to $p_\alpha(\alpha)d\omega' dA_s$. Let $a_f$ be the area of each facet. Then, the area of points in $dA_s$ that will reflect light from the direction $\theta_i$ into the solid angle $d\omega_r$ is equal to $(a_f P_\alpha(\alpha)d\omega' dA_s)$. All the reflecting facets are assumed to have the same local angle of incidence $\theta_i'$. Thus, the flux incident on the set of reflecting facets is determined to be

$$d^2\Phi_i = L_i d\omega_i (a_f p_\alpha(\alpha) d\omega' dA_s)\cos\theta_i'. \tag{3}$$

The fraction of incident light that is reflected by each planar face is determined by the Fresnel reflection coefficient $F'(\theta_i', \eta')$ [13]. Torrance and Sparrow have also considered the masking and shadowing effect on one microfacet by adjacent facets. Adjacent facets may obstruct either the flux incident on or the flux reflected by a given facet. In order to model these effects, they introduced the geometric attenuation factor $G(\theta_i, \theta_r, \phi_r)$. The obstruction of incident or reflected light depends on the angle of incident light and on the angle of reflection. Each facet is assumed to be one side of a V-groove cavity and to reflect light rays only once [15].

Taking the Fresnel reflection coefficient and the geometric attenuation factor into consideration, the flux $d^2\Phi_r$ reflected

into the solid angle $d\omega_r$ may be determined from the flux $d^2\Phi_i$ incident on the reflecting facets as

$$d^2\Phi_r = F'(\theta_i', \eta')G(\theta_i, \theta_r, \phi_r)d^2\Phi_i. \tag{4}$$

The radiance of specular component of the surface $dA_s$ in the direction $(\theta_r, \phi_r)$ is defined as

$$L_{spec,r} = \frac{d^2\Phi_r}{d\omega_r dA_s \cos\theta_r}. \tag{5}$$

Using (3) and (4), (5) can be rewritten as

$$L_{spec,r} = \frac{F'(\theta_i', \eta')G(\theta_i, \theta_r, \phi_r)L_i d\omega_i (a_f p_\alpha(\alpha) d\omega' dA_s)\cos\theta_i'}{d\omega_r dA_s \cos\theta_r}. \tag{6}$$

Only facets with normals that lie within the solid angle $d\omega'$ are capable of reflecting light into the solid angle $d\omega_r$. The relationship between these two solid angles is given as [11]

$$d\omega' = \frac{d\omega_r}{4\cos\theta_i'}. \tag{7}$$

Substituting (7) into (6), surface radiance of the surface $dA_s$ given by the specular component is given as

$$L_{spec,r} = L_i d\omega_i \frac{c a_f F'(\theta_i', \eta')G(\theta_i, \theta_r, \phi_r)}{4} \frac{1}{\cos\theta_r} \exp(-\frac{\alpha^2}{2\sigma_\alpha^2}). \tag{8}$$

Combining the Lambertian and specular components, Torrance and Sparrow gives the total radiance as

$$L_r = K_{lamb} L_i d\omega_i \cos\theta_i + K_{spec} L_i d\omega_i \frac{1}{\cos\theta_r} \exp(-\frac{\alpha^2}{2\sigma_\alpha^2}) \tag{9}$$

where $K_{lamb}$ determines the proportion of the incident energy that can be attributed to Lambertian factors, and $K_{spec}$ is given as

$$K_{spec} = \frac{c a_f F'(\theta_i', \eta')G(\theta_i, \theta_r, \phi_r)}{4}.$$

*Basic Image Irradiance Equation*

This paper will assume the following:

1) A1 — A sensor is far away from a surface patch; the imaging system can be modeled as an orthographic projection.[0]
2) A2 — A light source is far away from a surface patch; the illumination system can be modeled as a parallel ray illumination.
3) A3 — Incident angle $\theta_i$ and emitting angle $\theta_r$ are at most 60°; if the surface orientation is more inclined, we will discard the information from the patch.
4) A4 — Each region consists of one identical material; we can assume that reflectance parameters are constant over any given region.

[0] This assumption works well when we use a telephoto lens in the imaging system.

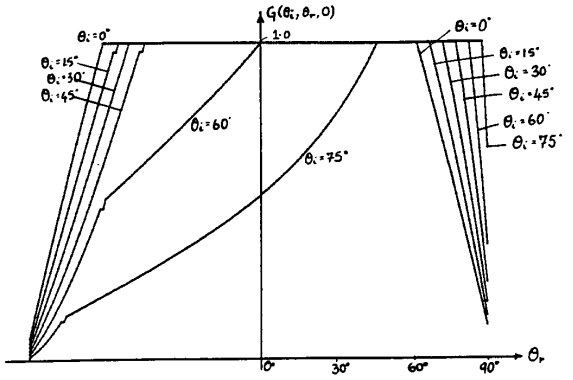


Fig. 2. Typical plot of geometric attenuation factor [11] .

Under these conditions, we will refine the Torrance-Sparrow reflectance model (e.g., (9)) into one that is more concise. We will then derive an image irradiance equation that we will use to predict the relationship between image Irradiance and surface reflectance.

The coefficient $K_{spec}$ contains the Fresnel coefficient and the geometric attenuation factor. Both of them depend on the illumination geometry. From metals and many other surfaces, it is observed that $F'$ has a nearly constant behavior until the local angle of incidence $\theta_i'$ approaches 90°. From assumption A3, we can assume that $F'$ is constant in our system.

Fig. 2 shows $G(\theta_i, \theta_r, 0)$ plotted as a function of $\theta_r$ for different values of $\theta_r$. We see that for angles of incidence not near the grazing angle, $G$ equals unity over an appreciable range of $\theta_r$. Again, from assumption A3, we can also assume $G = 1$ in our system.

The relationship between image irradiance $E$ and surface radiance $L_r$ is given as

$$E = L_r \frac{\pi}{4}(\frac{d}{f})^2 \cos^4\gamma \tag{10}$$

where $d$ is the diameter of the imaging lens, $f$ is the focal length of the lens, $\gamma$ is the angle between the optical axis and the line of sight [6].

If we are using orthographic projection, we can assume that $\gamma = 0$.[1] Thus, we can conclude that image irradiance is proportional to surface radiance and that this ratio is independent of the surface patch position.

Under these assumptions, we can derive the image irradiance equation from the Torrance-Sparrow reflectance model (see (9)):

$$E = E_l + E_s. \tag{11}$$

Image irradiance given by Lambertian reflection $E_l$ and that given by specular reflection $E_s$ can be described as

$$E_l = A\vec{S} \cdot \vec{N} \tag{12}$$

$$E_s = B\exp(-k\alpha^2)/N_z \tag{13}$$

[1] We will use a telephoto lens for our imaging system. In our setup, we will observe an object from 3 m away, where the field of view spans 30 cm. Thus, $\gamma = 0.05$ rad. $\cos^4\gamma = 0.995$.

where

$A$ – Lambertian strength constant,

$\vec{\mathbf{N}}$ – unit vector to represent surface orientation,

$\vec{\mathbf{S}}$ – unit vector to represent source direction,

$B$ – specular strength constant,

$\alpha$ – specular angle,

$k$ – specular sharpness,

$N_z$ – cosine of emitting angle,

and $A$, $B$, $k$, and $N_z$ can be described as

$$A = \frac{\pi}{4}(\frac{d}{f})^2 \cos^4\gamma d\omega_i L_i K_{lamb}$$
$$B = \frac{\pi}{4}(\frac{d}{f})^2 \cos^4\gamma \frac{c a_f F' G}{4} d\omega_i L_i$$
$$k = \frac{1}{2\sigma_\alpha^2}$$
$$N_z = \cos\theta_r.$$

The following section will recover these parameters using both a range image given by a range finder and a brightness image given by a TV camera.

## III. Parameter Estimation

This section will discuss a method for estimating reflectance parameters. We use the viewer-centered coordinate system rather than the Torrance-Sparrow local coordinate system. The viewer-centered coordinate system defines the viewer direction as its $Z$ axis. Its $x$ and $y$ axis agrees with the $x$ and $y$ axis of the image plane. In order to represent a pixel position in the image plane, we will use $(i, j)$. Since our camera model uses the orthographic projection, we can say that

$$x = s_x i,$$
$$y = s_y j,$$

where $s_x$ and $s_y$ are scale factors (see Fig. 3). On this coordinate system, the surface orientation and the source direction are denoted as $\vec{\mathbf{N}}(i,j)$ and direction by $\vec{\mathbf{S}}(i,j)$, respectively.

We will employ a two-step method to determine the reflectance parameters with the first step determining Lambertian strength $A$ and light source direction $\vec{\mathbf{S}}$ and the second step determining specular strength $B$ and specular sharpness $k$. In both steps, we will use the iterative least square fitting method.

### *Lambertian Parameters*

Let us consider the Lambertian component

$$E_l(i,j) = A(i,j)\vec{\mathbf{S}}(i,j) \cdot \vec{\mathbf{N}}(i,j). \tag{14}$$

Coefficient $A(i,j)$ depends both on the light source direction and on the light source's solid angle with respect to the position of the surface patch. The light source direction $\vec{\mathbf{S}}(i,j)$ also depends on the patch position. However, since we assume that the light source is far from the surface patch (A2), we can conclude that the light source direction is constant throughout the image. Under this assumption, we can consider its solid angle to be constant over the image. Thus, we can also conclude that strength of Lambertian component is constant throughout the image. Namely, $\vec{\mathbf{S}}$ and $A$ are constant throughout the image.

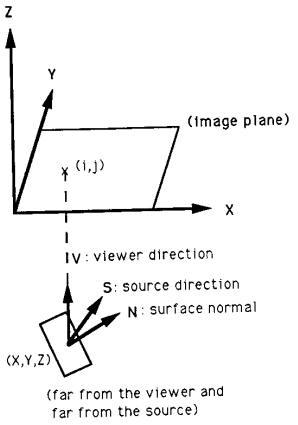


Fig. 3. Viewer-centered coordinate system and the orthographic projection.

Let us rewrite (14) into

$$\begin{aligned} E_l(i,j) &= A\vec{\mathbf{N}}(i,j) \cdot \vec{\mathbf{S}} \\ &= \vec{\mathbf{A}} \cdot \vec{\mathbf{N}}(i,j) \\ &= aN_x(i,j) + bN_y(i,j) + cN_z(i,j) \end{aligned} \tag{15}$$

where

$$\vec{\mathbf{N}}(i,j) = (N_x(i,j), N_y(i,j), N_z(i,j))^t$$
$$\vec{\mathbf{S}} = (S_x, S_y, S_z)^t$$
$$\vec{\mathbf{A}} = (a,b,c)^t$$
$$a = AS_x$$
$$b = AS_y$$
$$c = AS_z.$$

We will estimate the Lambertian strength and light source direction by performing the fitting calculation segmentation collection processes iteratively.

For the first iteration, we disregard the pixels' specular components. Since we can obtain $\vec{\mathbf{N}}(i,j)$ for each pixel by differentiating range values, we can determine $(a,b,c)$ by a least square fitting method. Namely, we find an $(a,b,c)$ that minimizes $e1$ over an object region as follows:

$$e1 = \sum_{i,j}(E(i,j)^{observed} - aN_x(i,j) - bN_y(i,j) - cN_z(i,j))^2 \tag{16}$$

where $E(i,j)^{observed}$ is the observed brightness value (image irradiance) recorded by a TV camera at pixel $(i,j)$, and $(N_x(i,j), N_y(i,j), N_z(i,j))$ is the surface orientation given by the range finder.

Once we obtain these parameters at the first iteration using all pixels, we can calculate ideal Lambertian brightness using

the parameters and surface orientations:

$$E_l^{calculated}(i,j) = \vec{\mathbf{A}}^* \cdot \vec{\mathbf{N}}(i,j)$$

where $\vec{\mathbf{A}}^*$ denotes the estimated $\vec{\mathbf{A}}$. Based on these calculated brightness values, we can decide the pixels that belong to Lambertian pixels:

**Criterion 1**: Extraction of Lambertian Pixel

1) $E(i,j)^{observed} - \vec{\mathbf{A}}^* \cdot \vec{\mathbf{N}}(i,j) > th$ — specular or interreflection pixel
2) $|E(i,j)^{observed} - \vec{\mathbf{A}}^* \cdot \vec{\mathbf{N}}(i,j)| < th$ — Lambertian pixel
3) $E(i,j)^{observed} - \vec{\mathbf{A}}^* \cdot \vec{\mathbf{N}}(i,j) < -th$ — shadow pixel.

Using this criterion, we will collect Lambertian pixels from an image. Using the collected Lambertian pixels, we repeat the fitting-calculation-segmentation-collection process.

We will repeat this process several times until $(a,b,c)$ converges. After the final convergence, the Lambertian strength $A$ and the light source $\vec{\mathbf{S}}$ can be obtained by the following formulas:

$$A = \sqrt{a^2+b^2+c^2}$$
$$\vec{\mathbf{S}} = (\frac{a}{A}, \frac{b}{A}, \frac{c}{A})^t.$$

*Specular Parameters*

Based on the light source direction $\vec{\mathbf{S}}$, we can determine the bisector direction between the source direction and the viewer direction $(0,0,1)$. The specular angle $\alpha(i,j)$ can be obtained as that between the surface orientation direction $\vec{\mathbf{N}}(i,j)$, the bisector direction of the viewer, and the source direction.

Criterion 1 will select brighter pixels, which consist of specular pixels and interreflection pixels. Based on this specular direction at each pixel, we will set up the following criteria:

**Criterion 2**: Extraction of Specular Pixels

1) $\alpha(i,j) \geq \alpha_0$ — interreflection pixel
2) $\alpha(i,j) < \alpha_0$ — specular pixel.

We will use this criterion to select the specular pixels.

We determine the specular parameters $B$ and $k$ by an iterative least square fitting method based on the specular pixels. A specular pixels' brightness value can be derived from the following equation:

$$d(i,j) = B\exp(-k\alpha(i,j)^2)/N_z(i,j)$$

where

$$d(i,j) = E(i,j) - \vec{\mathbf{A}} \cdot \vec{\mathbf{N}}(i,j).$$

In order to determine the parameters $B$ and $K$, we will employ a two-step fitting method. Assuming that $B$ (the specular strength) is known, the first step determines $K$ (the specular sharpness) so that it minimizes

$$e2 = \sum_{i,j}(\ln d^{observed}(i,j) + \ln N_z(i,j) - \ln B + 2K\alpha(i,j)^2)^2 \quad (17)$$

where $d^{observed}(i,j) = E^{observed}(i,j) - \vec{\mathbf{A}}^* \cdot \vec{\mathbf{N}}(i,j)$.

Then, based on the obtained $K$, the second step obtains $B$ so that it minimizes

$$e3 = \sum_{i,j}(d^{observed}(i,j) - B\exp(-k\alpha(i,j)^2)/N_z(i,j))^2. \quad (18)$$

We will repeat these two steps (17) and (18) several times until the two parameters $B$ and $K$ converge; $B$ and $K$ stop moving.

It is possible to obtain $B$ and $K$ simultaneously so that they minimize (17). However, due to the logarithm fitting, this method gives erroneous $B$. On the other hand, if we minimize (18), we have to employ a nonlinear fitting method. Thus, we employ the two-step fitting method mentioned above.

In order to start the above-mentioned method, we need an initial value for $B$. For the pixels that satisfy $\alpha = 0$, $d$ has the maximum value $d(i,j) = B$. We use this maximum value of $d(i,j)$ as the initial approximation of $B$.

## IV. Determining Threshold Values

We will estimate reflectance parameters using the criterion summarized as follows:

**Criterion 3**: Segmentation Summary

1) $E(i,j)^{observed} - \vec{\mathbf{A}}^* \cdot \vec{\mathbf{N}}(i,j) > th$
   a. $\alpha(i,j) \geq \alpha_0$ — interreflection pixel
   b. $\alpha(i,j) < \alpha_0$ — specular pixel
2) $|E(i,j)^{observed} - \vec{\mathbf{A}}^* \cdot \vec{\mathbf{N}}(i,j)| < th$ — Lambertian pixel
3) $E(i,j)^{observed} - \vec{\mathbf{A}}^* \cdot \vec{\mathbf{N}}(i,j) < -th$ — shadow pixel.

This criterion contains two threshold values: the Lambertian $th$ and the specular $\alpha_0$. We will determine these threshold values based on the fluctuations of range and brightness values.

*Threshold Value for Lambertian Pixel th*

To fix the threshold value, we have to estimate the random fluctuations of the quantity $|E(i,j)^{observed} - \vec{\mathbf{A}}^* \cdot \vec{\mathbf{N}}^{observed}(i,j)|$. The fluctuations $\delta E'$ can be described as

$$\delta E' = \delta E + \vec{\mathbf{A}}^* \cdot \delta\vec{\mathbf{N}}. \quad (19)$$

The fluctuations $\delta E$ depend on the TV camera; it is assumed that they follow a Gaussian distribution with zero mean and standard deviation $\sigma_E$. We obtain its standard deviation by examining the outputs of our TV camera.

The fluctuations in the surface orientation $\delta\vec{\mathbf{N}}$ can be obtained by examining the conversion method from a measured range value $z$ to a surface orientation.

Our range finder provides three images $(X(i,j), Y(i,j), Z(i,j))$, which indicate the world coordinate system of the pixel $(i,j)$. Using this, we can obtain the gradient of that pixel by the following formulas:

$$p(i,j) = \left.\frac{\partial Z}{\partial X}\right|_{i,j} = \frac{Z(i+1,j) - Z(i-1,j)}{X(i+1,j) - X(i-1,j)}$$
$$q(i,j) = \left.\frac{\partial Z}{\partial Y}\right|_{i,j} = \frac{Z(i,j+1) - Z(i,j-1)}{Y(i,j+1) - Y(i,j-1).} \quad (20)$$

The fluctuations in surface orientation $(\delta p, \delta q)$ can be estimated from the fluctuations in a range value $z$ as

$$\delta p = \frac{\delta z}{\epsilon_1}$$
$$\delta q = \frac{\delta z}{\epsilon_2} \tag{21}$$

where $\epsilon_1 = \frac{X(i+1,j)-X(i-1,j)}{2}$ and $\epsilon_2 = \frac{Y(i,j+1)-Y(i,j-1)}{2}$. Here, we ignore the fluctuations in $(X, Y)$ measurements.

Then, the angle between the surface orientation and the light source direction $\theta$ can be obtained from the surface orientation $(p, q)$, where we assume that the light source direction is $(0.0, 0.0)$ for simplicity:

$$\theta = \tan^{-1}\sqrt{p^2+q^2}.$$

Thus

$$\delta\theta = \frac{\partial\theta}{\partial p}\delta p + \frac{\partial\theta}{\partial q}\delta q,$$
$$= \frac{1}{1+p^2+q^2}\frac{1}{\sqrt{p^2+q^2}}(p\delta p + q\delta q). \tag{22}$$

Since $\vec{\mathbf{A}}\cdot\delta N = A\sin\theta\delta\theta$, inserting $\sin\theta = \frac{\sqrt{p^2+q^2}}{\sqrt{1+p^2+q^2}}$ (21) and (22) into (19), we obtain

$$\delta E' = \delta E + m\delta z \tag{23}$$

where

$$m = 2(\frac{A}{\epsilon})l,$$
$$l = \frac{p^2+q^2}{(1+p^2+q^2)^{1.5}},$$
$$\epsilon = min[\epsilon_1, \epsilon_2].$$

We will assume that the fluctuations of the observed range value are modeled as a Gaussian distribution with zero mean and standard deviation $\sigma_z$. Namely, $\delta z \sim N(0, \sigma_z)$. We will obtain its standard deviation by examining the output of our range finder. As mentioned before, we assumed $\delta E \sim N(0, \sigma_E)$. Using the theorem for the sum of the two Gaussian distributions, we can model $\delta E'$ as $N(0, \sigma_{E'})$:

$$\sigma_{E'} = \sqrt{\sigma_E^2 + (m\sigma_z)^2}. \tag{24}$$

We will use $3\sigma_{E'}$ as the threshold value for Lambertian pixels, namely, $th = 3\sigma_{E'}$.

*Threshold Value for Specular Pixels $\alpha_0$*

We will determine the threshold value $\alpha_0$ to decide whether one pixel is specular or not. The brightness of the specular component is denoted as $B\exp(-k\alpha^2)/N_z$. We will consider the range of $\alpha$ to be the range of significant specular angles, such that those angles give more than 20% of the maximum specular component:

$$\exp(-k\alpha_0^2) = 0.2. \tag{25}$$

We employ the threshold value as $\alpha_0$, which is given by

$$\alpha_0^2 = -\frac{1}{k}\ln 0.2. \tag{26}$$

The value of $\alpha_0$ depends on the value of $k$. We cannot determine $k$ value before calculating the specular parameters. Thus, at the first iteration, we will use an initial threshold value. For the initial threshold value, we use $\alpha_0 = 0.3$. For the second and later iterations, we will use the exact threshold value given by (26).

## V. Experiments

This section examines the recoverability of parameters by our method. We conduct several experiments using synthesized and real images. The purpose of the experiments using synthesized images is to examine the convergence of our system to the true value under various noise levels. The purpose of the experiments using real images is to examine the applicability of our system to real problems.

*Recovering Lambertian Parameters from Synthesized Images*

This subsection will examine the recoverability of Lambertian parameters by our method using synthesized brightness and range images under various noise levels.

We generate synthesized brightness images of a Lambertian sphere, $A = 200$, $B = 0$, and $\vec{\mathbf{S}} = (0.0, 0.0, 1.0)$ under three noise levels: $\sigma_E = 0, 3, 6$ (see Fig. 4). We also generate the synthesized range images under three noise levels: $\sigma_z = 0, 1.59, 3.17$. Here, our system, which is described later on, has the noise level of $\sigma_E = 3$ and $\sigma_z = 1.59$.

We use $3\sigma_{E'}$ as the threshold value $th$ for the Lambertian pixel in Criterion 3. $\sigma_{E'}$ as given by (24), contains three parameters $A$, $l$, and $\epsilon$. The value $A$ depends on the gain of a TV camera. This experiment uses $A = 200$. The parameter $\epsilon$ depends on the image resolution of a TV camera. Examining $x$ values of two adjacent pixels of our system gives $\epsilon = 26$.

We assumed that the maximum inclined angle is 60° (A3). Under this range of surface orientations, $-1.73 \leq p, q \leq 1.73$, $l$ takes $-0.384 \leq l \leq 0.384$. Thus, we employ the maximum value of $l$ as the $l$ value in the above equation; $l = 0.4$. Inserting these parameters, we obtain the threshold values shown in Table I at three noise levels in brightness (row) and range measurement (column). The contents of the table give the actual threshold values to be used.

The synthesized images are given to our parameter recovery program using the threshold values. The light source direction $\vec{\mathbf{S}}$ is obtained correctly in all cases; the error is less than 0.01% with respect to $(0.0, 0.0, 1.0)$. The Lambertian strength $A$ is estimated as shown in Table II. Since the noise-free case, there is no interval given by the theoretical threshold ((24) gives zero for $\theta$), we use the threshold value given by $\sigma_E = 3$ and $\sigma_z = 0$. Even in the extremely noisy case such that both the TV camera and range finder has twice the larger noise level $\sigma_E = 6, \sigma_z = 3.17$, our program still converges the true albedo value.

*Recovering Lambertian and Specular Parameters from Synthesized Images*

This subsection examines the recoverability of Lambertian and specular parameters under several noise levels using synthesized images.

Criterion 3 contains two threshold values $th$ and $\alpha_0$ for recovering Lambertian and specular parameters. For the Lam-

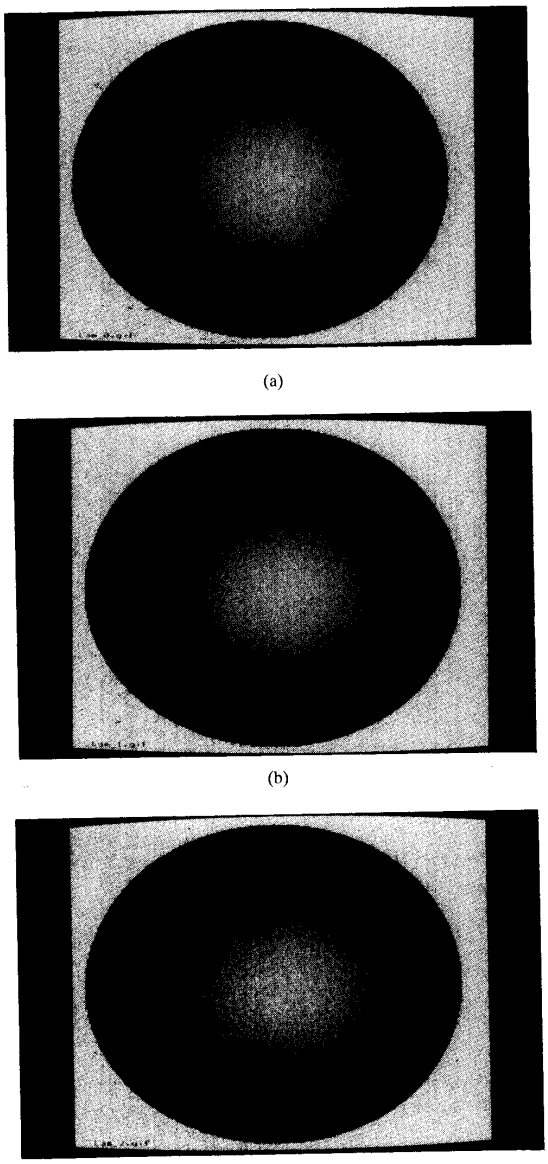

(a) (b) (c)

Fig. 4. Synthesized brightness images at three noise levels: (a) $\sigma_E = 0$; (b) $\sigma_E = 3$; (c) $\sigma_E = 6$.

bertian threshold $th$ we use the values in Table I.

The specular threshold value $\alpha_0$ depends on the specular sharpness $k$. At the initial iteration, we use 0.3. At the later iterations, we use $\alpha_0$ such that they satisfy $\exp(-k\alpha_0^2) = 0.2$.

Fig. 5 denotes synthesized images of $A = 125$, $\vec{\mathbf{S}} = (0.0, 0.0, 1.0)$, $B = 125$, and $k = 20$ under three noise levels: $\sigma_E = 0, 3, 6$. Fig. 6 denotes those of $A = 125$, $\vec{\mathbf{S}} = (0.0, 0.0, 1.0)$, $B = 125$, and $k = 10$, and Fig. 7 denotes those of $A = 125$, $\vec{\mathbf{S}} = (0.0, 0.0, 1.0)$, $B = 125$, and $k = 5$. The range images are the same ones used in the previous experiments.

TABLE I
THRESHOLD VALUES AT VARIOUS NOISE LEVELS

| | | $\sigma_z$ | | |
|---|---|---|---|---|
| | | 0 | 1.59 | 3.17 |
| $\sigma_E$ | 0 | 0 | 12 | 24 |
| | 3 | 6 | 13 | 25 |
| | 6 | 12 | 17 | 27 |

TABLE II
RECOVERED LAMBERTIAN STRENGTH VALUES $A$

| | | $\sigma_z$ | | |
|---|---|---|---|---|
| | | 0 | 1.59 | 3.17 |
| $\sigma_E$ | 0 | 200 | 200 | 199 |
| | 3 | 200 | 200 | 199 |
| | 6 | 200 | 200 | 199 |

These images are given to our parameter recovery program using the threshold value in Table I and $\alpha_0 = 0.165$ for $k = 20$, $\alpha_0 = 0.407$ for $k = 10$, and $\alpha_0 = 0.638$ for $k = 5$, respectively.

The algorithm to determine the specular parameters consists of two steps of the least fitting methods: obtaining K using a known B and obtaining B using a known K. From these experiments, it turned out that the method to obtain the B value from the specular direction is accurate and stable, and it is not necessary to perform the second least square fitting method. Thus, we only perform the first step of the least square fitting using the B value estimated from the specular direction and do not perform the second step.

Tables III, IV, and V show the obtained parameters for $k = 20$, $k = 10$, and $k = 5$, respectively. The light source direction $\vec{\mathbf{S}}$ is again obtained correctly in all cases; the error is less than 0.01% with respect to $(0.0, 0.0, 1.0)$.

In order to examine the effect of the relative strength of the parameters, we perform simulations under various combinations of strength parameters. In these experiments, we fix the noise level as $\sigma_E = 3$ and $\sigma_z = 1.59$. Tables VI, VII, and VIII show the results. The light source direction $\vec{\mathbf{S}}$ is obtained correctly in all cases.

From these experiments, we can conclude the following:

1) Under larger $k$ values, the system can recover the $k$ value, as well as other parameters, correctly.[2]
2) Under smaller $k$ values, more dull specular reflection, and greater noise levels, it becomes more difficult to obtain the correct $k$ value.
3) Under smaller $k$ values, the estimated Lambertian strength $A$ is sensitive to the threshold value.[3]

[2] One of the representative $k$ values, which the Torrance-Spparow model holds, is $k \approx 10$ (or $C \approx 0.05$ [15] ).

[3] The second and third points are due to the reason that our algorithm implicitly assumes that the majority of pixels do not contain any significant amounts of the specular component. Under smaller $k$ values, where this assumption is not valid, we may have to introduce some robust fitting procedures.

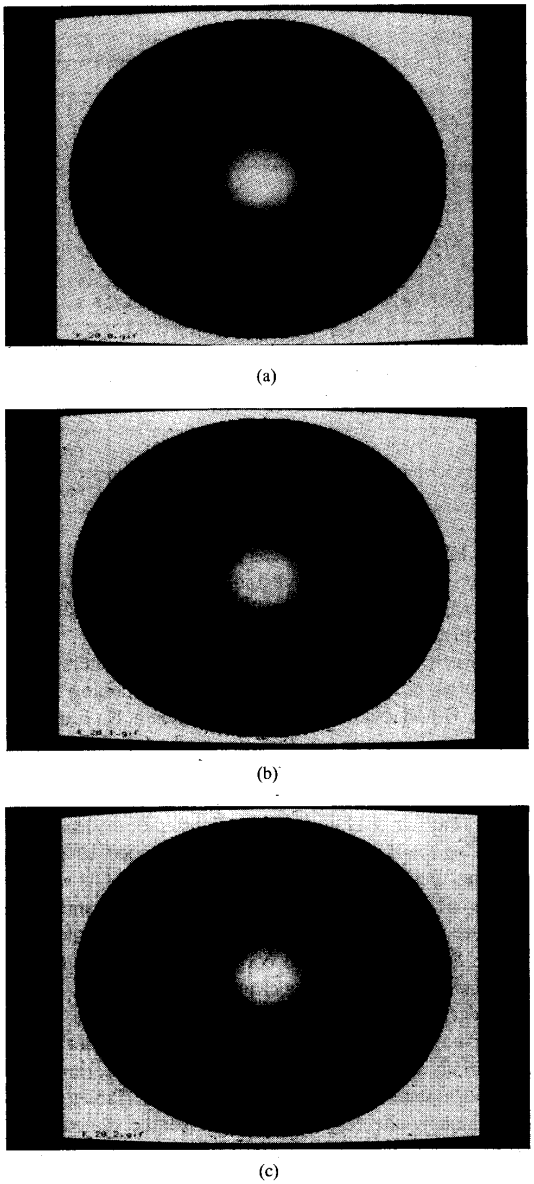

Fig. 5. Synthesized brightness images of $A = 125$, $\vec{\mathbf{S}} = (0.0, 0.0, 1.0)$, $B = 125$, and $k = 20$ under three noise levels: (a) $\sigma_E = 0$; (b) $\sigma_E = 3$; (c) $\sigma_E = 6$.

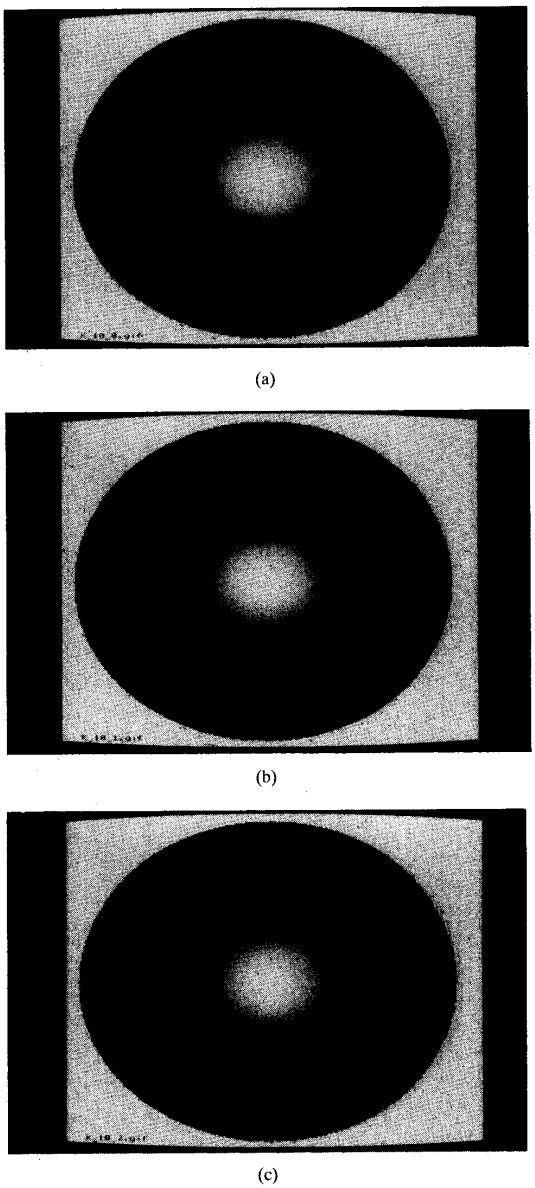

Fig. 6 Synthesized brightness images of $A = 125$, $\vec{\mathbf{S}} = (0.0, 0.0, 1.0)$, $B = 125$ and $k = 10$ under three noise levels; (a) $\sigma_E = 0$; (b) $\sigma_E = 3$; (c) $\sigma_E = 6$.

*Recovering Reflectance Parameters from Real Images*

This subsection will examine the performance of our system on several real images to evaluate the accuracy of our system. Fig. 8 shows our hardware system,[4] which consists of a slide projector (Procabin 67-2) with a liquid crystal shutter, a CCD TV camera (Sony model xc-57 with a 12.5–75 mm Cosmicar zoom lens), and a point light source. Our current setup has the base line length of 16 cm. We usually place an object 2–3 m away from the system.

Input brightness from a standard CCD camera has $\gamma$ characteristics. In order to compensate for this, we will construct a linearization look-up table using a color chart. Input brightness is linearized by using this table.

Our range finder provides three images $X(i,j), Y(i,j), Z(i,j)$ that indicate the world coordinate system of the pixel $(i,j)$. Using this, we can obtain the gradient of that pixel $(p(i,j), q(i,j))$ by using (20).

[4] This system was originally developed at Osaka University [12]. It is currently manufactured by Osaka Gas Information Systems, Osaka, Japan, and is available as a commercial product (the RFX 4 system).

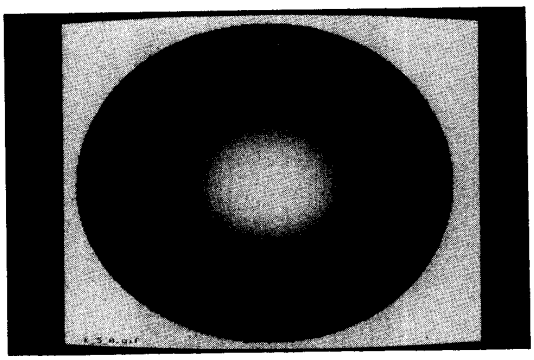

(a)

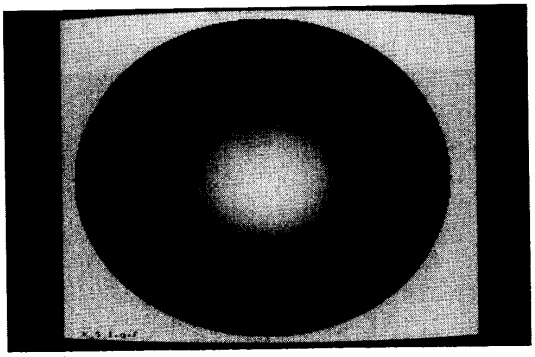

(b)

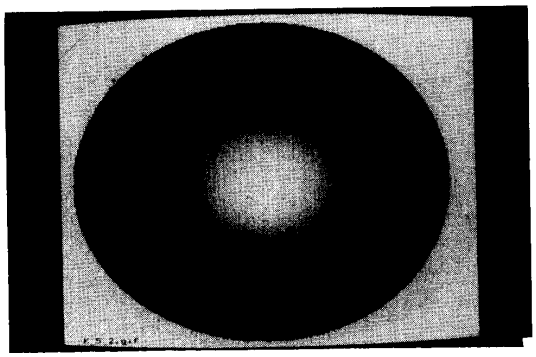

(c)

Fig. 7. Synthesized brightness images of $A = 125$, $\vec{\mathbf{S}} = (0.0, 0.0, 1.0)$, $B = 125$ and $k = 5$ under three noise levels; (a) $\sigma_E = 0$; (b) $\sigma_E = 3$; (c) $\sigma_E = 6$.

Using this, we can get a surface normal from the following equations:

$$N_x(i,j) = p(i,j)/\sqrt{p(i,j)^2 + q(i,j)^2 + 1}$$
$$N_y(i,j) = q(i,j)/\sqrt{p(i,j)^2 + q(i,j)^2 + 1}$$
$$N_z(i,j) = 1/\sqrt{p(i,j)^2 + q(i,j)^2 + 1}. \quad (27)$$

We need the fluctuations of brightness and range measurements. From the experiments, we obtain that the brightness distribution of our TV camera has $\sigma_E = 3$.

TABLE III
RECOVERED REFLECTANCE PARAMETERS $A$=125, $B$=125, $K$=20

| | | $K$=20 | | |
|---|---|---|---|---|
| | | $\sigma_z$ | | |
| | | 0 | 1.59 | 3.17 |
| $\sigma_E$ | 0 | $A$=125<br>$B$=124<br>$K$=20 | $A$=126<br>$B$=124<br>$K$=21 | $A$=128<br>$B$=123<br>$K$=21 |
| | 3 | $A$=127<br>$B$=124<br>$K$=20 | $A$=127<br>$B$=124<br>$K$=22 | $A$=128<br>$B$=125<br>$K$=21 |
| | 6 | $A$=129<br>$B$=121<br>$K$=21 | $A$=128<br>$B$=1124<br>$K$=22 | $A$=128<br>$B$=124<br>$K$=20 |

TABLE IV
RECOVERED REFLECTANCE PARAMETERS $A$=125, $B$=125, $K$=10

| | | $K$=10 | | |
|---|---|---|---|---|
| | | $\sigma_z$ | | |
| | | 0 | 1.59 | 3.17 |
| $\sigma_E$ | 0 | $A$=126<br>$B$=124<br>$K$=10 | $A$=130<br>$B$=122<br>$K$=11 | $A$=133<br>$B$=121<br>$K$=11 |
| | 3 | $A$=131<br>$B$=123<br>$K$=11 | $A$=131<br>$B$=123<br>$K$=11 | $A$=134<br>$B$=122<br>$K$=11 |
| | 6 | $A$=134<br>$B$=121<br>$K$=11 | $A$=134<br>$B$=122<br>$K$=11 | $A$=134<br>$B$=123<br>$K$=11 |

TABLE V
RECOVERED REFLECTANCE PARAMETERS $A$=125, $B$=125, $K$=5

| | | $K$=5 | | |
|---|---|---|---|---|
| | | $\sigma_z$ | | |
| | | 0 | 1.59 | 3.17 |
| $\sigma_E$ | 0 | $A$=131<br>$B$=120<br>$K$=5 | $A$=141<br>$B$=114<br>$K$=6 | $A$=150<br>B=109<br>$K$=6 |
| | 3 | $A$=142<br>$B$=115<br>$K$=6 | $A$=144<br>$B$=114<br>$K$=6 | $A$=151<br>$B$=110<br>$K$=6 |
| | 6 | $A$=153<br>$B$=111<br>$K$=6 | $A$=155<br>$B$=108<br>$K$=6 | $A$=156<br>$B$=112<br>$K$=6 |

In order to determine the fluctuations of range values, we measure the range values of pixels on a white board using our range finder. After having obtained the equation of the board, we examine the residues of subtracting range values calculated by the equation from those observed. Then, we conclude that our range finder has $\sigma_z = 1.59$. Based on these two values and consulting Table I, we obtain $th = 13$.

*Real Lambertian Object:* Fig. 9(a) shows a Lambertian object: a salad bowl painted with Krylon flat white 1502 paint.

TABLE VI
RECOVERED REFLECTANCE PARAMETERS
$K$=20, UNDER $\sigma_E$=3 AND $\sigma_z$=1.59

| | | $K$=20 | | |
|---|---|---|---|---|
| | | $A$ | | |
| | | 62 | 125 | 250 |
| $B$ | 62 | $A$=64<br>$B$=61<br>$K$=21 | $A$=127<br>$B$=61<br>$K$=21 | $A$=252<br>$B$=62<br>$K$=21 |
| | 125 | $A$=64<br>$B$=123<br>$K$=22 | $A$=127<br>$B$=124<br>$K$=22 | $A$=255<br>$B$=124<br>$K$=22 |
| | 250 | $A$=65<br>$B$=247<br>$K$=21 | $A$=127<br>B=248<br>$K$=21 | $A$=252<br>$B$=249<br>$K$=21 |

TABLE VII
RECOVERED REFLECTANCE PARAMETERS
$K$=10, UNDER $\sigma_E$=3 AND $\sigma_z$=1.59

| | | $K$=10 | | |
|---|---|---|---|---|
| | | $A$ | | |
| | | 62 | 125 | 250 |
| $B$ | 62 | $A$=67<br>$B$=60<br>$K$=11 | $A$=130<br>$B$=60<br>$K$=11 | $A$=255<br>$B$=61<br>$K$=11 |
| | 125 | $A$=68<br>$B$=122<br>$K$=11 | $A$=130<br>$B$=123<br>$K$=11 | $A$=255<br>$B$=123<br>$K$=11 |
| | 250 | $A$=69<br>$B$=247<br>$K$=10 | $A$=131<br>$B$=246<br>$K$=10 | $A$=255<br>$B$=248<br>$K$=11 |

TABLE VIII
RECOVERED REFLECTANCE PARAMETERS
$K$=5, UNDER $\sigma_E$=3 AND $\sigma_z$=1.59

| | | $K$=5 | | |
|---|---|---|---|---|
| | | $A$ | | |
| | | 62 | 125 | 250 |
| $B$ | 62 | $A$=78<br>$B$=53<br>$K$=6 | $A$=140<br>$B$=56<br>$K$=6 | $A$=265<br>$B$=54<br>$K$=6 |
| | 125 | $A$=82<br>$B$=113<br>$K$=6 | $A$=144<br>$B$=114<br>$K$=6 | $A$=268<br>$B$=115<br>$K$=6 |
| | 250 | $A$=87<br>$B$=234<br>$K$=6 | $A$=148<br>$B$=235<br>$K$=5 | $A$=272<br>$B$=237<br>$K$=5 |

Fig. 9(b) shows a needle image of the object obtained from a range image by our system.

From these images, we obtain $A = 105$ and $\vec{\mathbf{S}} = (0.028, 0.019, 0.999)$. In order to evaluate these results, we plot the distribution of brightness values with respect to the angle between the light source and the surface orientation $\theta_i$. The abscissa of Fig. 10(a) denotes the angle $\theta_i$. The ordinate

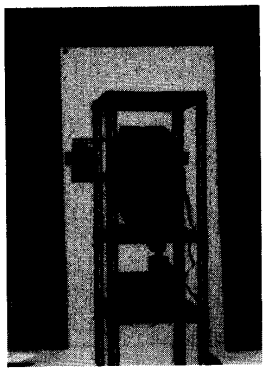

Fig. 8. Liquid crystal (OGIS) range finder and point light source.

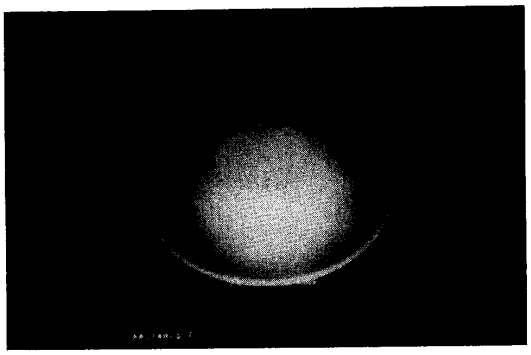

(a)

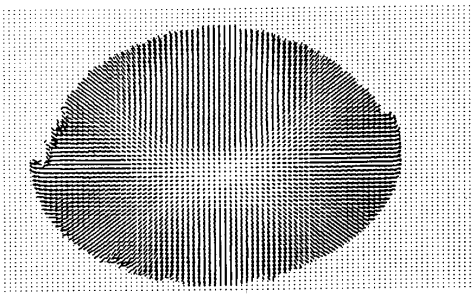

(b)

Fig. 9. Lambertian object: (a) Input brightness distribution; (b) needle image obtained from the range image given by our system.

of the figure denotes the brightness. The thin points indicate the observed brightness, whereas the thick line indicates the calculated brightness:

$$E = A\,\vec{\mathbf{S}} \cdot \vec{\mathbf{N}} = A \cos\theta_i.$$

In order to evaluate the error distribution, we calculate ideal brightness values at each pixel by $E(i,j) = A\,\vec{\mathbf{N}}(i,j) \cdot \vec{\mathbf{S}}$. Fig. 10(b) shows the calculated ideal brightness distribution. Fig. 10(c) shows the difference between the calculated and original brightness. In this experiment, the residue of brightness is

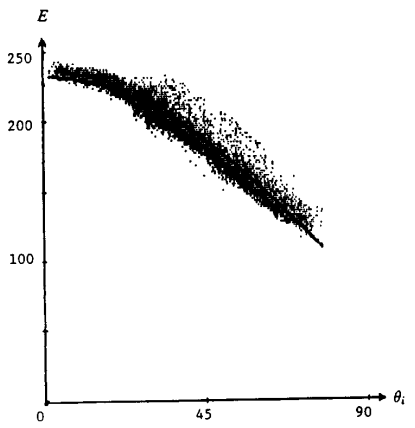


(a)

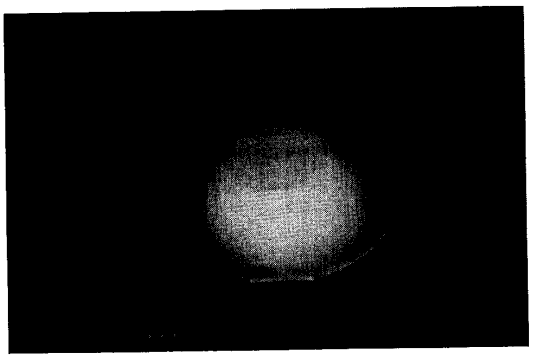

(b)

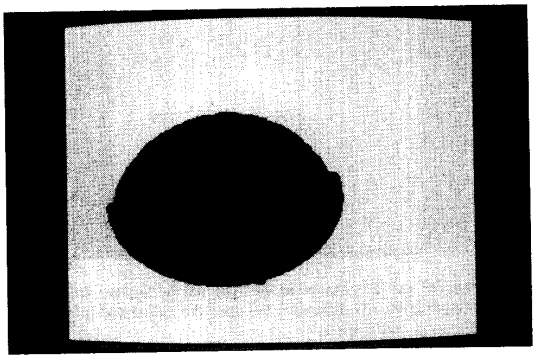

(c)

Fig. 10. Result of a Lambertian object: (a) Brightness plot. The abscissa denotes the angle between the light source direction and the surface orientation. The ordinate denotes the brightness. The thin points indicate observed brightness, whereas the thick line indicates the calculated brightness; (b) calculated brightness distribution; (c) difference between the calculated brightness and observed brightness distribution. Roughly, no errors exist.

small, and we do not proceed to the second step to obtain specular parameters.

*Real Specular Object:* Fig. 11(a) shows a specular object: a salad bowl painted with Sears bright silver 66578 paint. Fig. 11(b) shows the needle image of the object.

We first examine Lambertian parameters $A$ and $\vec{\mathbf{S}}$. Since

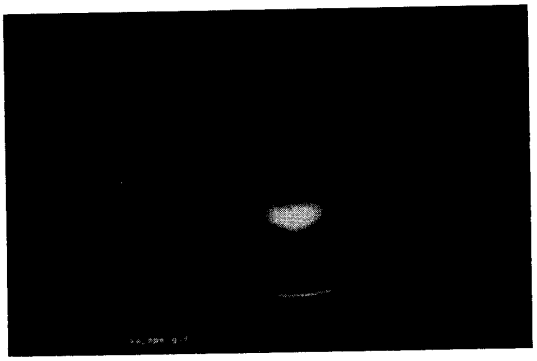

(a)

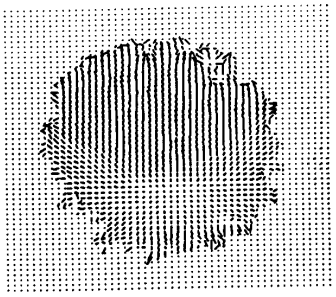

(b)

Fig. 11. Specular object: (a) Brightness image; (b) needle image.

this object has little Lambertian component, the light source direction is unstable. Thus, we use the light source direction given in the the previous experiment (0.028, 0.019, 0.999). We neglected the Lambertian strength $A = 0$.

Fig. 12(a) shows the result. The abscissa denotes the square of the angle between the surface orientation and the bisector of the light source and the TV camera direction $\alpha^2$. The ordinate denotes $\ln d + \ln N_z$. The thin points indicate observed values, whereas the thick line indicates $\ln B + K\alpha^2$, where the specular parameters are $B = 134, k = 11$. Fig. 12(b) shows the the brightness distribution obtained using the parameters $B\frac{\exp(-k\alpha^2)}{N_z}$. Fig. 12(c) shows the difference between the calculated and original brightness distribution.

*Real Tomato:* Fig. 13 shows an image of a real tomato taken in our system. By applying our method to the tomato, we obtain $A = 34$, $\vec{\mathbf{S}} = (-0.059, -0.039, 0.997)$, $B = 89$, $k = 9$. In this case, the light source direction is slightly erroneous.

By using these parameters, we obtain the brightness distribution and then make the difference between the calculated and original brightness distribution.

This $k$ value is smaller than expected. This is probably because the tomato has a transparent skin, and reflection also occurs under the transparent skin.

## VI. Building A System To Recover Reflectance Parameters Of Human Faces

This section overviews the system that obtains the reflectance parameters of a human face.

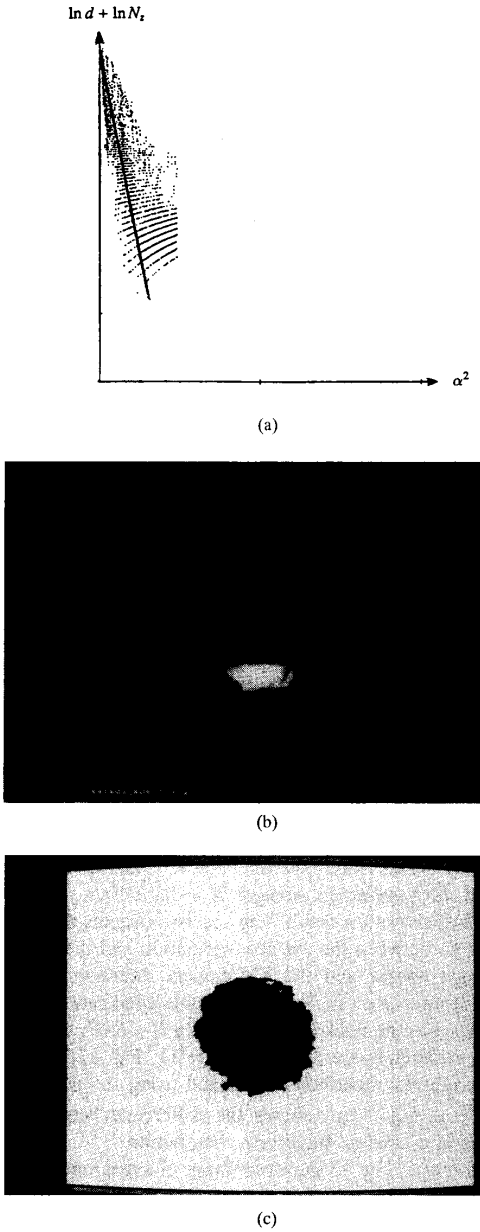


Fig. 12 (a) Brightness distribution. The abscissa denotes square of specular angles $\alpha^2$. The ordinate denotes $\ln d + \ln N_s$. The thin points indicate observed values, whereas the thick line indicates $\ln B + K\alpha^2$, where $B = 134, k = 10.8$; (b) calculated brightness distribution; (c) difference between the calculated brightness and original brightness distribution.

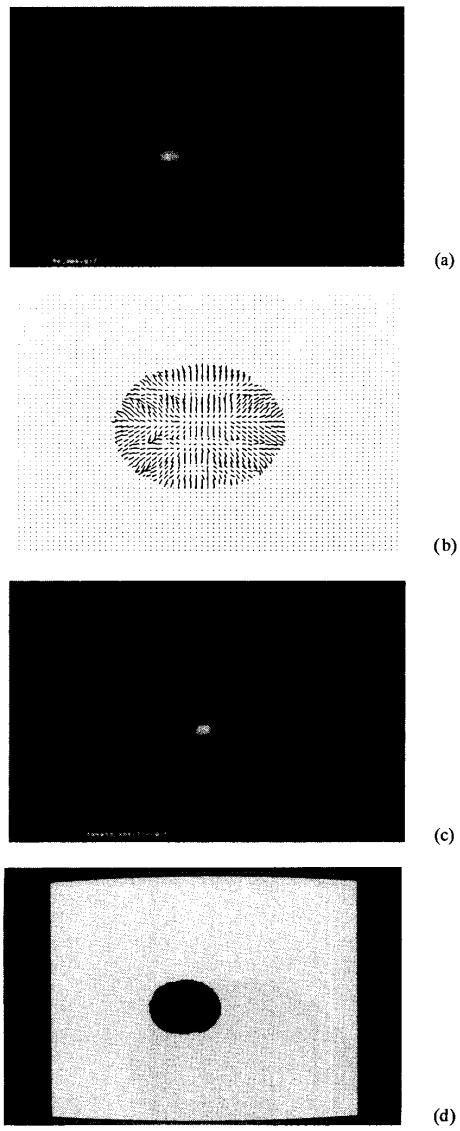


Fig. 13. Tomato: (a) Brightness image; (b) needle image; (c) calculated brightness distribution; (d) difference between the calculated brightness and original brightness distribution.

Fig. 14 shows the software configuration. From a range image, given by a range finder, and a brightness image, given by a standard TV camera, we will obtain the following three items: a needle image, an object area, and a normalized brightness image. The normalized brightness is obtained in the same method as described in the subsection on Recovering Reflectance Parameters from Real Images. We will then use these items to determine reflectance parameters. Using the reflectance parameters, we will segment images into three kinds of pixels: Lambertian pixel, specular pixel, and shadow pixel. The system will also reconstruct ideal images such as a Lambertian image or a specular image using these parameters.

Fig. 15(a) shows the input brightness image, and (b) shows the range image obtained by our range finder.

We have to extract the face area from the background. We ask a person to sit down so that his/her face is located roughly at the center of the image. Thus, based on the range values at the central area and the rough dimension of a face, we will threshold the range image. Next, we execute a connectivity

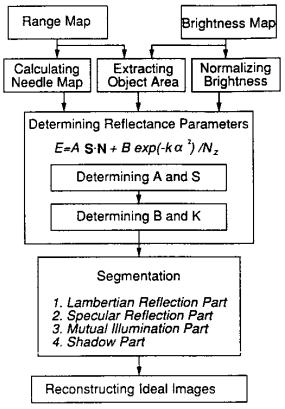


Fig. 14. Software configuration.

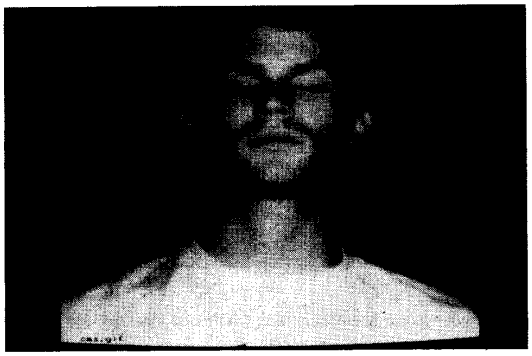

(a)

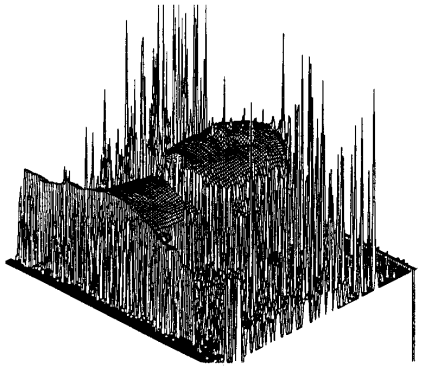

(b)

Fig. 15. Input images: (a) Brightness image; (b) range image.

analysis to group pixels into regions. We then decide that the largest central region will be the face region. Fig. 16(a) shows the extracted face region, whereas Fig. 16(b) shows the needle image over the extracted face region.

We will estimate reflectance parameters based on the method described in Section III. First, we estimate Lambertian strength $A$ and the light source direction $\vec{\mathbf{S}}$. Second, we estimate specular strength $B$ and specular sharpness $k$. For this example, we

(a)

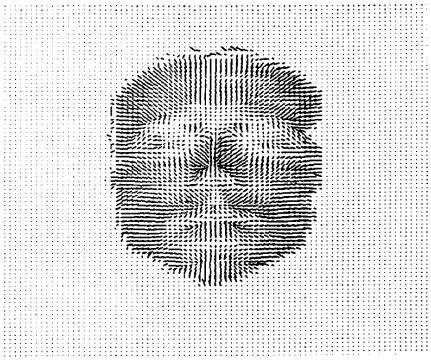

(b)

Fig. 16. Face extraction: (a) Extracted face region; (b) extracted needle image over the face region.

obtain $A = 103, S = (0.021, 0.049, 0.999), B = 27, k = 7$. Using these parameters, we can segment the input image into three parts: Lambertian, specular, and shadow. Fig. 17 shows the segmentation results.

We can reconstruct an ideal image, which consists of either only Lambertian pixels or specular pixels using reflectance parameters. For a Lambertian reflection image consisting of all Lambertian pixels, we use

$$E(i,j) = A^* \vec{\mathbf{N}}(i,j) \cdot \vec{\mathbf{S}}^*. \tag{28}$$

Here, estimated Lambertian strength $A^*$ and estimated light source direction $\vec{\mathbf{S}}^*$ are given from the analysis, and $\vec{\mathbf{N}}(i,j)$ is given from the needle image. Since we know the range information, we can reconstruct a side face from a frontal face.

For a specular reflection image consisting of all specular pixels, we use

$$E(i,j) = B^* \exp(-k^* \alpha(i,j)^2)/N_z(i,j) \tag{29}$$

where $B^*$ (specular strength) and $k^*$ (specular sharpness) are given from the analysis, and $\alpha(i,j)^2, N_z(i,j)$ are given from the needle image.

Fig. 18 shows a Lambertian image, and Fig. 19 shows a specular image.

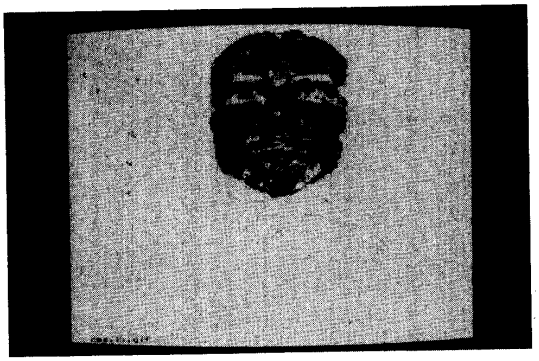

(a)

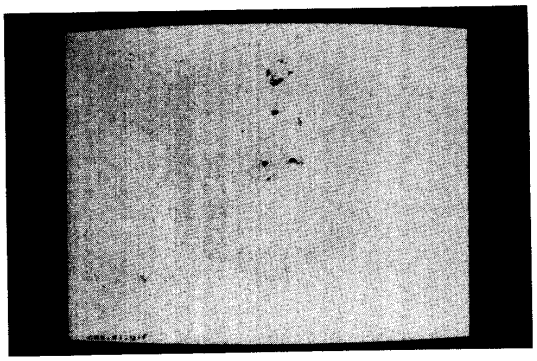

(b)

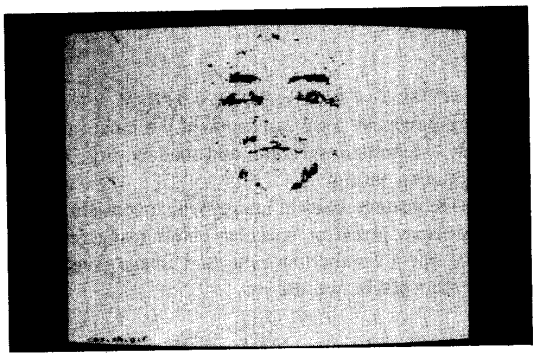

(c)

Fig. 17. Segmentation result: (a) Lambertian pixel; (b) specular pixel; (c) shadow pixel.

## VII. Conclusion

This paper discusses a method that analyzes reflectance parameters derived from a range image and a brightness image. Our system employs the Torrance-Sparrow model as the basic reflectance model. We refined this model into a more specific model and derived an image irradiance equation. This equation consists of four reflectance parameters: Lambertian strength, light source direction, specular strength, and specular sharpness.

By iteratively using a least square fitting method, we extracted these four parameters from a range image, which was given by a range finder, and a brightness image, which was given by a TV camera. Using the reflectance parameters, we segmented input images into four parts: Lambertian reflection, specular reflection, interreflection, and shadow parts. We also reconstructed ideal images that consist of only Lambertian or specular reflection.

(a)

(b)

Fig. 18. Reconstructed Lambertian face: (a) Frontal face; (b) side face.

By recovering the reflectance parameters from the surface of an object, we can extract both sharpness and the ratio between Lambertian and specular strength from the original image. This recognition of surfaces makes it possible to assign objective and concrete criteria by which an object should be recognized or evaluated rather than being forced to rely on the less precise judgement of human inspection.

One application of this process may be the evaluation of fruit that might be found in a packing shed. The second application may be delineating the different regions found in the human face; this information could be used by cosmetics companies offering individualized make-up or face-care schemes.

## Acknowledgment

T. Kanade and R. Reddy provided many useful comments and encouragement. K. Porsche and F. Solomon proofread drafts of this paper and provided many useful comments that have improved the readability of this paper. C. M. Sundius and Y. Mei helped us to develop some of the software.

(a)

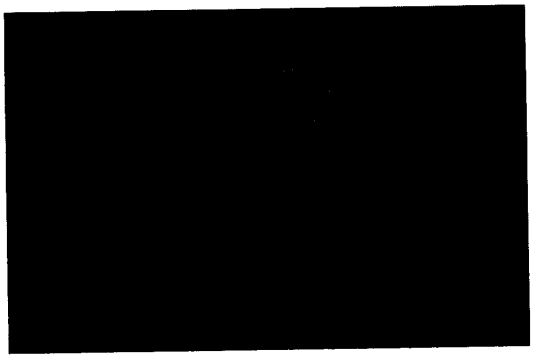

(b)

Fig. 19. Reconstructed specular face: (a) Frontal face; (b) side face.

The authors also thank S. Nayar, H. Sato, Y. Fujiwara, and the members of the Task-Oriented Vision Laboratory, School of Computer Science, Carnegie Mellon University, for their valuable comments and suggestions.

## REFERENCES

[1] P. Beckmann and A. Spizzichino, *The Scattering of Electromagnetic Waves from Rough Surfaces*. London: Pergamon, 1963.
[2] P. J. Besl, "Range imaging sensors," Tech. Rep. GMR-6090, Comput. Sci. Dept., GM Research Laboratories, Warren, MI, Mar. 1988.
[3] J. F. Blinn, "Models of light reflection for computer synthesized picture," *Comput. Graphics*, vol. 11, pp. 192–198, 1977.
[4] R. L. Cook and K. E. Torrance, "A reflectance model for computer graphics," *Comput. Graphics*, vol. 15, no. 3 pp. 307–316, Aug. 1981.
[5] G. Healey and T. O. Binford, "Local shape from specularity," *Comput. Vision Graphics Image Processing*, vol. 42, pp. 62–86, 1988.
[6] B. K. P. Horn and R. W. Sjoberg, "Calculating the reflectance map," Tech. Rep. AI Memo 498, Mass. Inst. Technol., Artificial Intell. Lab., Oct. 1978.
[7] A. F. Houchens and R. G. Hering, "Bidirectional reflectance of rough metal surfaces," in G. B. Heller, Ed., *Themophysics of Spacecraft and Planetary Bodies*. New York: Academic, 1967, pp. 65–89.
[8] G. J. Klinker, S. A. Shafer, and T. Kanade, "The measurement of highlights in color image," *Int. J. Comput. Vision*, vol. 2, no. 1, 1988.
[9] J. H. Lambert, *Photometria sive de mensura de gratibus luminis colorum et umbrae*. Augsburg: Eberhard Klett, 1960.
[10] S. K. Nayar, K. Ikeuchi, and T. Kanade, "Extracting shape and reflectance of Lambertian, specular, and hybrid surfaces, "Tech. Rep. CMU-RI-TR-88-14, Carnegie Mellon Univ., Robotics Inst., Aug. 1988.
[11] ——, "Surface reflection: Physical and geometrical perspectives," *IEEE Trans. Patt. Anal. Machine Intell.*, vol. 13, no. 7, pp. 611–634, July 1991.
[12] K. Sato, H. Yamamoto, and S. Inokuchi, "Range imaging system utilizing nematic liquid crystal mask," in *Int. Conf. Comput. Vision*(London), 1987, pp. 657–661.
[13] R. Siegel and J. R. Howell, *Thermal Radiation Heat Transfer*. New York: McGraw-Hill, 1972.
[14] H. D. Tagare and R. J. deFigueiredo, "A framework for the construction of general reflectance maps for machine vision," Tech. Rep., Rice Univ., Dept. of Elec. Comp. Eng., 1989.
[15] K. E. Torrance and E. M. Sparrow, "Theory for off-specular reflection from roughened surfaces," *J. Optical Soc. Amer.*, vol. 57, pp. 1105–1114, Sept. 1967.
[16] L. B. Wolff, "Using polarization to separate reflection components, in *Proc. IEEE Conf. Comput. Vision Patt. Recognition*, 1989, pp. 363–369.
[17] R. J. Woodham, "Reflectance map techniques for analyzing surface defects in metal castings," Tech. Rep. AI-TR-457, Mass. Inst. Technol., Artificial Intell. Lab., Cambridge, MA, 1978.

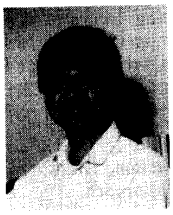

**Katsushi Ikeuchi** (M'78) received the B. Eng. degree in mechanical engineering from Kyoto University, Kyoto, Japan, in 1973 and the M. Eng and Ph.D. degrees in information engineering from the University of Tokyo, Tokyo, Japan, in 1975 and 1978, respectively.

Since then he has held research positions at the Artificial Intelligence Laboratory, Massachusetts Institute of Technology, Cambridge, and the Electrotechnical Laboratory, Ministry of International Trade and Industry, Japan. In 1986, he joined the School of Computer Science, Carnegie Mellon University. He currently holds the position of senior research scientist. His research accomplishments in image understading include the development of "smoothness constraints," where neighboring points have similar surface orientations, by which he recovered shape from shading and shape from texture, iteratively. He also pioneered the use of specular reflections to recover surface orientations. Instead of discarding specular reflections, he actively used them to recover shape and reflectance. He has also developed several vision systems. In 1983, he developed a bin-picking system based on photometric stereo, which is a method that recovers surface orientations using structured lighting; he also developed the extended Gaussian image, which is a spatial histogram of surface orientations. After joining Carnegie Mellon University, he has been developing a vision algorithm compiler that converts an object and sensor model into a vision program automatically. This work has spawned a large body of further research such as object modeling, sensor modeling, strategy generation, and program conversion, as well as aplications.

Dr. Ikeuchi received the D. Marr best paper award in 1990 at the International Conference of Computer Vision and Pattern Recognition and certificates for outstanding contributions in 1986 at the SME World Conference on Robotics Research.

**Kosuke Sato** (M'89) received the B.E., M.E., and Ph.D. degrees in engineering from Osaka University in 1983, 1985, and 1988, respectively.

He is currently a research associate in the Department of Control Engineering at Osaka University, Osaka, Japan. From 1988 to 1990, he was a visiting research scientist in the Robotics Institute at Carnegie Mellon University. His research interests include 3-D range imaging, scene understanding, and sensory fusion for computer vision.

Dr. Sato is a member of the IEEE Computer Society.